

Article

A Study of Recirculating Flow Fields Downstream of a Diverse Range of Axisymmetric Bluff Body Geometries Suitable for Flame Stabilization

Georgios Paterakis, Konstantinos Souflas , Andreas Naxakis and Panayiotis Koutmos *

Laboratory of Applied Thermodynamics, Department of Mechanical Engineering and Aeronautics, University of Patras, 26504 Patras, Greece; paterakis.gio@gmail.com (G.P.); souflaskonstantinos@gmail.com (K.S.); andreasnaxakis@upatras.gr (A.N.)

* Correspondence: koutmos@mech.upatras.gr

Abstract: This work investigates the non-reacting time averaged and fluctuating flow field characteristics downstream of a variety of axisymmetric baffles, operating in combination with an upstream double-cavity premixer arrangement. The study aims to broaden knowledge with respect to the impact of different bluff body shapes, leading and trailing edge flow contours, blockage ratios and incoming flow profiles impinging on the bluff body, on the development and properties of the downstream recirculating wake. Particle Image Velocimetry (PIV) measurements have been employed to obtain the mean and turbulent velocity fields throughout the centrally located recirculation zone and the adjacent developing toroidal shear layer. The results are helpful in demarcating the cold flow structure variations in the near wake of the examined baffles which support and, to some extent, determine the flame anchoring performance and heat release disposition in counterpart reacting configurations. Additionally, such results could also assist in the selection of the most suitable flame stabilization configuration for fuels possessing challenging combustion behavior such as multi-component heavier hydrocarbons, biofuels, or hydrogen blends.

Keywords: central recirculation zone; bluff body stabilizers; PIV; turbulent flow fields



Citation: Paterakis, G.; Souflas, K.; Naxakis, A.; Koutmos, P. A Study of Recirculating Flow Fields Downstream of a Diverse Range of Axisymmetric Bluff Body Geometries Suitable for Flame Stabilization. *Aerospace* **2021**, *8*, 339. <https://doi.org/10.3390/aerospace8110339>

Academic Editor: Pietro Catalano

Received: 13 October 2021

Accepted: 6 November 2021

Published: 10 November 2021

Publisher's Note: MDPI stays neutral with regard to jurisdictional claims in published maps and institutional affiliations.



Copyright: © 2021 by the authors. Licensee MDPI, Basel, Switzerland. This article is an open access article distributed under the terms and conditions of the Creative Commons Attribution (CC BY) license (<https://creativecommons.org/licenses/by/4.0/>).

1. Introduction

The turbulent flow downstream of a bluff body is of fundamental interest to combustion applications for the assessment of flame anchoring techniques as well as to the aerodynamic design of structural elements of airborne or ground devices [1–4]. Bluff bodies are an important ingredient, alone or in combination with a swirler, in flame stabilization devices. The flow distribution downstream of a bluff body geometry affects flame placement and has a significant impact on the combustion stability, efficiency and emissions. Its flow dynamic characteristics also play a crucial role in the development of the turbulent properties of the adjacent wake. Further understanding of bluff body wake aerodynamics and its implications in flame stabilization performance can be provided by mapping the topology of the flow field under non-reacting conditions.

As a consequence, numerous experimental and computational works have been devoted to provide further insight into the aerodynamic design properties, wake flow topologies, turbulence characteristics, inert mixing disposition and time-dependent flow behavior in a diversity of bluff shapes e.g., [5–9]. These works focused on the examination of the isothermal recirculating bluff body flow fields, either with regard to a counterpart reacting set up e.g., [10–12] or as part of the aerodynamic design of structural elements e.g., [13,14].

Regarding the combustion applications, the majority of these studies has, so far, concentrated on comparing global properties and turbulent characteristics in the baffle's wake, between cold and reacting flows, with particular emphasis placed on configurations

pertaining to, either diffusion e.g., [5,15–17] or fully premixed combustion applications e.g., [8,18–20].

More recent investigations have been extended on variants of the usual geometry set-ups in an effort to accommodate studies of partially premixed or stratified inlet fuel–air mixture stabilization arrangements [21–30]. Such concepts have been under intensive investigation because they offer an attractive and flexible alternative that improves and promotes the lean premixed combustion concept, which is more frequently used in practical combustion systems. The majority of the previously reported studies on bluff body flow and flame stabilization has focused on examining stand-alone bluff geometries placed against a cross flow [6,27,31–35].

In the present study, we extend the previously reported in the literature, standard, isolated bluff body configuration by introducing a further complexity regarding the influence of the pre-conditioning of the flow approaching the bluff body under study, as has been demonstrated in [36]. Specifically, here we address the non-reacting flow performance of commonly used bluff body stabilizers operating in combination with an upstream fuel–air premixing module which, in various forms, represents a configuration frequently encountered in practical systems. In such partially premixed arrangements the aero-thermodynamic coupling between the integrated fuel–air premixer section and the individual baffle stabilizer itself, plays a functional role in the overall wake development and stabilization properties [12,30,37,38].

Within this context, the aim of the present effort is to perform a systematic and parametric investigation of the performance of a variety of axisymmetric afterbody baffle shapes, operated in conjunction with a preceding upstream premixing arrangement, similar to the one described in [12,30,37,38], that facilitates regulation of the flow and mixing profiles that supply the bluff body wake. The turbulent flow, within this upstream fuel–air premixer, is interacting with the actual stabilizer flow characteristics, controlling the level and shape of flow and mixture inhomogeneities at the inlet to the main combustion zone as well as its dispositions across the anchoring region. A number of studies has focused on the cold flow and reacting characteristics downstream of the currently investigated premixer arrangement, combined solely with a disk shaped baffle, operated over a range of inlet mixture conditions. These respective investigations concentrated on the study of the scalar mixing properties for different baffle shapes [38] and on the reacting properties with or without the impact of swirl [11,24,37,39], under stratified or fully premixed inlet mixture conditions. Additionally, investigations regarding the effect of both stratification and preheat on the reacting front have been presented in [12,30,40], while in [41] the authors have discussed the influence of acoustic modulation of the incoming velocity and equivalence ratio gradient on the combustion zone.

Nevertheless, the non-reacting flow fields downstream of a wider range of baffles, have not been previously explicitly examined or discussed. Therefore, the current cold flow study represents an independent parametric investigation of a diverse range of bluff body shapes, which are here coupled to an upstream premixer, double cavity section, with the objective to evaluate individual operating features that strongly affect anchoring, flame stabilization and downstream wake development in a counterpart reacting set up.

Important operating characteristics are the trailing edge aerodynamics, the entrainment capability, the recirculation strength, the turbulence intensity along the reacting front and the mean and turbulent strain field near the flanks of the recirculation where the anchoring region most usually resides. Studies under isothermal conditions are of great value despite the alterations that may be induced by the reactions and can crucially assist in the delineation of optimum selections amongst the multiplicity of possible stabilizer combinations during the early stages of burner design. Along these lines, and also based on the combustion properties of the employed reacting fuel mixture, such as flame speeds, ignition delays, extinction stretches and diffusional behaviors, one can identify the most convenient baffle candidate for efficient flame stabilization.

Two dimensional particle image velocimetry (PIV) measurements of these isothermal flows have been carried out to provide detailed mean and fluctuating velocity fields and allow the evaluation of global and turbulent structural flow properties in the near wake of a range of premixer/bluff body shapes.

The presented data and analysis, combined with information from previous works e.g., [38], aims at providing a systematic and extensive description of the cold flow and mixing characteristics for the range of investigated baffles. The measurements could also be suitably exploited for the assessment of simulation methodologies and turbulence models. Additionally, such results could also be useful in the improvement of flame stabilization procedures of alternative fuels, biofuels or hydrogen blends which present distinct and challenging combustion features.

2. Experimental Methodology

The experimental facility is shown in Figure 1 and described in detail in [37,38]. Three axisymmetric baffles (A, B, C) connected along their axis with a 10 mm hollow tube comprise the premixer/burner arrangement. The premixer section consists of the disk shaped bluff bodies “B” and “C” with a diameter of 25 mm and thicknesses of 7.5 and 5.3 mm respectively. This premixer section was designed to promote fuel–air premixing and to produce a radial equivalence ratio (Φ) gradient, as shown in Figure 1 and described in detail in [38]. The stabilizing afterbody “A” is either a disk- (D) or cone- (C) shaped body, with a diameter of 25 or 36 mm (D_b) and a rim thickness of either 3.5, 7.5 or 15 mm (RIM1, 2, 3 respectively), Figure 1.

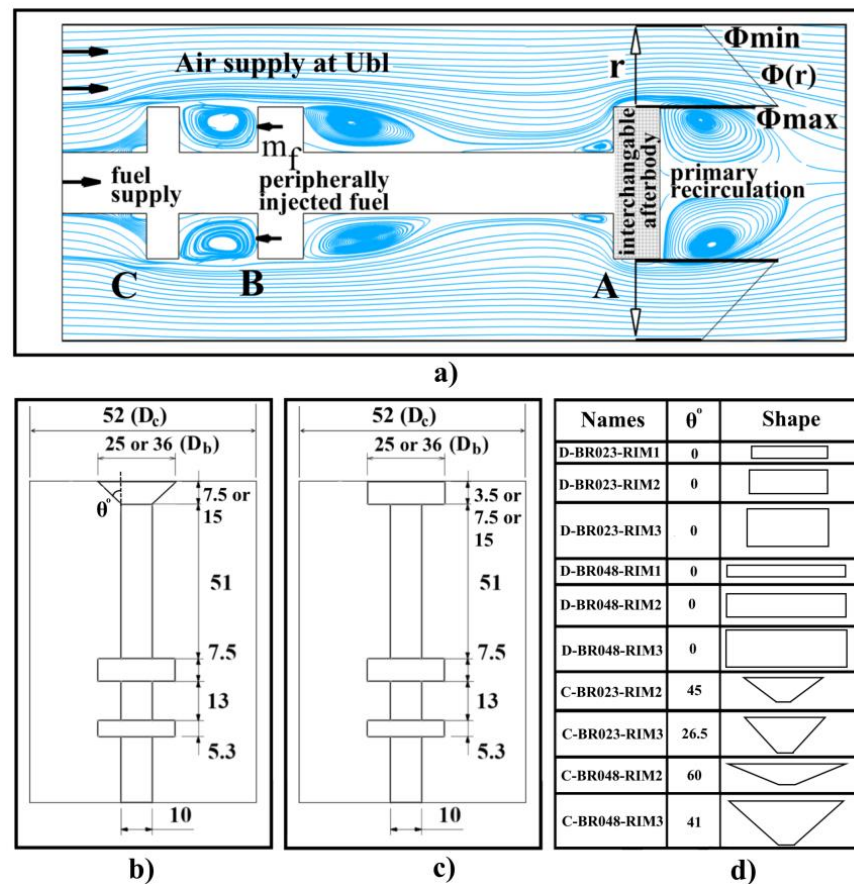


Figure 1. Premixer/burner configurations, (a) flow patterns of premixer/burner set up, (b) cone shaped after-body premixer/burner set up, (c) disk shaped after-body premixer/burner set up, (d) investigated after-bodies.

For the air supply measurement, an orifice plate, designed and built according to ISO 5167 guidelines, has been employed. A differential pressure manometer, Furness Controls (FCO520 AirPro), has been used to measure the pressure drop, with an accuracy of 0.25% of the reading value at 600 Pa. The overall accuracy of the measuring system has been estimated at about 2.5% [41]. Bulk, blocked velocities, at the annular afterbody exit plane (U_{bl}) varied from 6.60 to 10.2 m/s, resulting in Reynolds numbers from 1100 to 16,000. The bulk velocity was calculated at the annular exit plane of as: $U_{bl} = \frac{\dot{m}}{\rho_f A}$, where \dot{m} is the air mass flow rate at the exit plane, ρ_f is the density of the fluid and A is the annular area of the exit plane. The air mass flow rate has been kept constant for all investigated cases. The specific mass flow rate has been chosen in order to be safely within the turbulent regime and be consistent with previously reported works. The fuel injection location, although not used in the current flow field investigations, it is included in Figure 1 to provide a complete overview of the premixer/burner configuration. The resulting radially stratified fuel–air mixture profile at the annular exit plane of the burner is discussed in [38].

3. Diagnostic Tools and Experimental Methods

Particle Image Velocimetry

Measurements of the velocity field have been conducted with a two-dimensional particle image velocimetry configuration (2DPIV, LaVision® FlowMaster 2D, (LaVision GmbH, Göttingen, Germany)) as has also been described in detail in [12,38]. Briefly, the system comprised of a 15 mJ QUANTEL EVERGREEN® double-pulsed Nd:YAG laser (Quantel by LUMIBIRD, Lannion, France) at 532 nm, producing a light sheet of 0.5 mm thickness, and a LaVision® Imager Pro X 2M CCD camera (LaVision GmbH, Göttingen, Germany). The timing of the whole system was regulated through a LaVision® Programmable Timing Unit (PTU 9), (LaVision GmbH, Göttingen, Germany). The camera resolution was at 1600×1200 pixels and was coupled with an AF Micro Nikkor 60 mm lens (f/4), (Nikkor by Nikon Corporation, Tokyo, Japan). The camera lens was equipped with an interference filter centered at 532 nm with bandwidth of 10 nm, full width at half maximum, to isolate the laser beam. The sampling rate of the system was at 10 Hz and 800 image pairs were recorded for each investigated case. The chosen number of pictures has been shown to be sufficient for converged averages and root-mean-square (RMS) velocity analyses as described in detail in [42]. The captured investigation area was 66.80 mm by 51.72 mm, resulting in a spatial resolution of about $42 \mu\text{m}/\text{pixel}$. Each velocity vector was calculated after a “multipasses with overlap” cross-correlation algorithm application. In the initial step, two passes at 64×64 pixel interrogation window and 50% overlap were performed and subsequently a pass at 32×32 pixel interrogation window and 75% overlap was applied resulting into a final spatial resolution of about $0.334 \text{ mm}/\text{vector cell}$. The main airflow was seeded with TiO_2 particles, with nominal mean diameter of $5 \mu\text{m}$, a relaxation time up to $\tau \approx 3 \times 10^{-4}$ s and a maximum Stokes number of 0.19. Therefore, it can be argued that that tracing accuracy errors can be up to 1% [38]. Particles were supplied to the main air flow through four inlets at a distance of 500 mm upstream the exit plane to ensure the homogenization of the stream. The seeding system consisted of an air compressor, two air–filters, OMI QF and HF, to remove oil particles up to a diameter of $0.1 \mu\text{m}$ from the air, a particle seeder and a chiller dryer in order to exclude any humidity in the seeding stream and avoid any agglomeration of the particles. The area of interest downstream of the burner was confined with a 300×300 mm square cross section chamber, allowing optical view for the laser beams and the camera employed. The uncertainty estimation procedure has been presented and discussed in detail in [38] and the derived values, for the cases investigated here, are provided in Appendix A.

4. Investigated Bluff Body Geometries

Time averaged and fluctuating flow characteristics have been measured for a series of bluff body configurations. Both disk (D) and conical (C) afterbody geometries have been employed with a thickness of 3.5 (RIM1), 7.5 (RIM2) or 15 mm (RIM3). For

each variant two different diameters have been assessed corresponding to blockage ratios ($BR = (D_b/D_c)^2$) of 0.23 and 0.48. The geometrical characteristics of the various, interchangeably investigated afterbodies are summarized in Figure 1.

The range of the above bodies can stabilize either fully premixed or stratified inlet mixture flame configurations. The isothermal scalar (fuel–air) mixing fields of the studied baffles, Figure 1, have been thoroughly investigated and discussed in [38]. The current parametric study focuses on the velocity and turbulence flow characteristics downstream from these afterbody geometries and supplements the fuel–air mixing field details presented in [38]. The combined data sets allow for a more complete and comprehensive assessment of the characteristics of the non-reacting flows produced by the above range of baffles which are likely candidates for use as flame stabilizers, burning a variety of fuels. The possible extent of the flow field diversification that can be obtained is discussed below.

5. Results and Discussion

Figure 2 depicts the overall mean flow structure of the recirculation zone for two stabilizer configurations, D-BR023-RIM2 and C-BR0.23-RIM2. The 2D streamline plots of the axial (u) and radial (v) velocity vectors are superimposed over the time-averaged axial velocity contour fields, illustrating the toroidal shear layers and the disposition of the near wake recirculation regions.

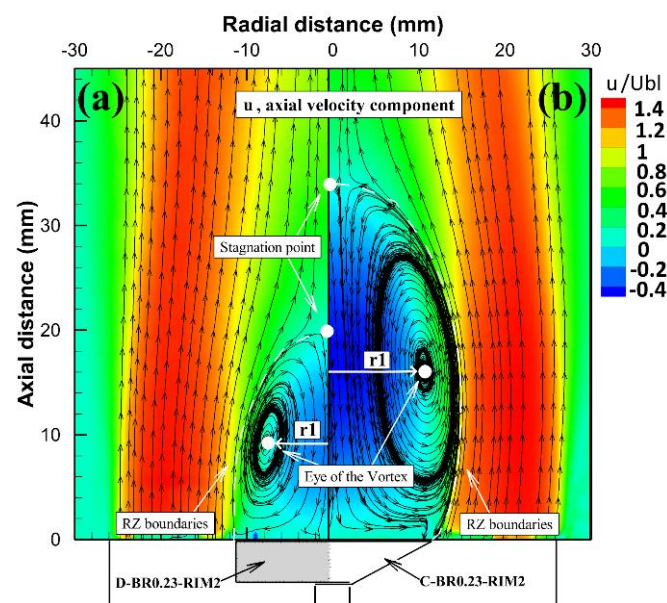


Figure 2. Structure of recirculation zone (RZ) and longitudinal velocity component disposition for (a) D-BR023-RIM2 and (b) C-BR0.23-RIM2 cases.

The zero or stagnation streamline is also depicted by the white dashed line, which demonstrates the recirculation zone boundary. It extends from the rim edge of the baffle up to the reattachment point, where the air flow converges toward the stagnation point along the centerline. Based on these boundaries the length and width of the recirculation zone can be determined. The illustrated recirculation zone features follow similar dispositions for the remaining of the investigated afterbody baffles with quantitative differences mainly encountered with regard to the extent, formation and strength of the reverse flow zone, as indicated in Figure 3.

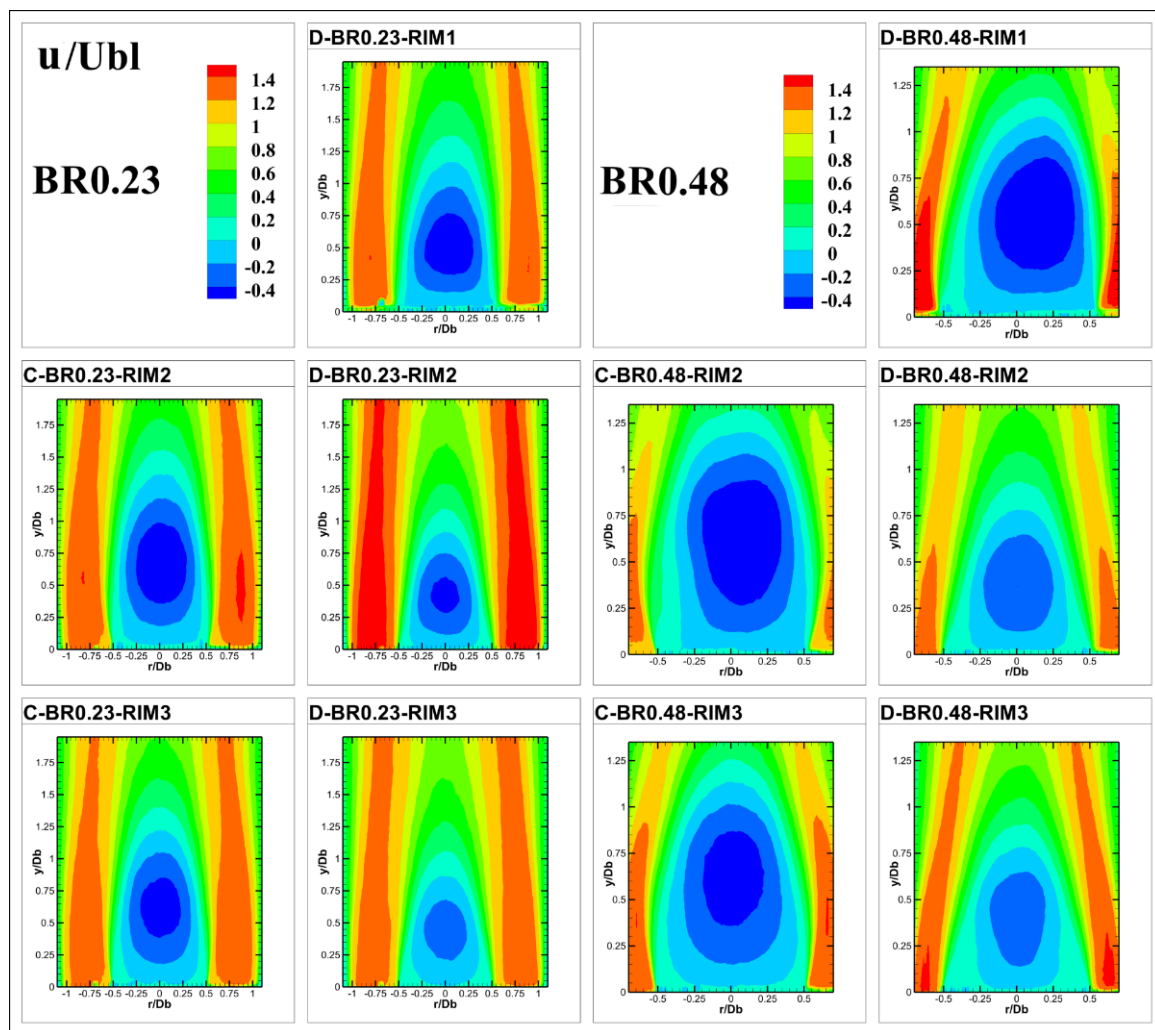


Figure 3. Normalized time averaged axial velocity field.

Figure 3 displays the non-dimensional mean axial velocity distributions for all investigated cases. Bluff body shape and blockage ratio variations result in modifications of the geometrical characteristics of the reverse flow envelope. Cone shaped bluff bodies, and particularly those with the steeper angle, form larger recirculation zones than the disk-shaped ones, as a result of the larger deflection angle of the flow issuing at their trailing edge, with an attendant longer and wider reverse flow zone. It was also noticed that in the case of the thin rim disk (D-BR0.48-RIM1), the recirculation zone exhibited an asymmetric behavior, as also observed in [43]. An increase in the thickness of the disk rim shortened the recirculation zone bubble by about 15% for BR0.23 and 25% for BR0.48 and moderately reduced back flow velocities, retarding the RZ strength. Additionally, thicker baffles proved more capable at maintaining a symmetric wake development regardless of the blockage ratio.

The stagnation points for D-BR0.23-RIM2 and D-BR0.23-RIM3 were located close to $y/D_b = 0.9$, whereas, for the thinner disk, D-BR0.23-RIM1 and the cone, C-BR0.23-RIM3, the reattachment was encountered at about $y/D_b = 1.2$. For C-BR0.23-RIM2 the recirculation zone length was extended up to $y/D_b = 1.34$. Specifically, thicker disks produced shorter lengths (of about $0.77 D_b$) than the thinner disk ($1.03 D_b$). Moreover, the RZ of disk-shaped baffles was reduced compared to the C-BR0.48-RIM2 ($1.17 D_b$) and C-BR0.48-RIM3 ($1.14 D_b$) cases, Table 1. Finally, an increase in BR values, for the disk shaped bluff bodies, notably lengthens the RZ by 22% for RIM2, 19.5% for RIM3 and 11% for RIM1 case, a trend implying a diminishing impact of blockage on the narrower disks.

Table 1. Operational characteristics of the investigated cases and important global features of recirculation zone.

Name	U _{bl} (m/s)	U _{rec,max} /U _{bl}	X _{rec,max} /D _b	$\frac{\dot{m}_{REC}}{\dot{m}_{inlet}}$ %	L/D _b	W/D _b	L/W	Trailing Edge Angle (°)
C-BR023-RIM2	6.66	0.55	0.67	6.58	1.34	1.19	1.13	19.00
C-BR023-RIM3	6.66	0.50	0.61	5.34	1.22	1.10	1.11	18.00
D-BR023-RIM1	6.66	0.51	0.51	5.64	1.16	1.17	0.99	18.50
D-BR023-RIM2	6.77	0.39	0.44	2.98	0.92	0.98	0.94	−3.00
D-BR023-RIM3	6.77	0.31	0.44	2.41	0.86	0.96	0.90	−2.00
C-BR048-RIM2	10.20	0.55	0.63	21.96	1.17	1.21	0.97	32.00
C-BR048-RIM3	10.20	0.54	0.65	15.94	1.14	1.16	0.98	25.00
D-BR048-RIM1	10.20	0.63	0.51	23.24	1.03	1.16	0.89	34.00
D-BR048-RIM2	10.04	0.39	0.32	8.45	0.77	0.96	0.79	−4.00
D-BR048-RIM3	10.05	0.36	0.43	4.25	0.76	0.95	0.81	−5.00

In overall, coned shaped bluff bodies produced longer RZ lengths than disks, i.e., ranging from 41 to 45% for BR0.23 and 48 to 53% for BR0.48 independently of the bluff body thickness. It should also be mentioned that the off-axis placement of the reattachment position for D-BR0.48-RIM1 baffle at $(r/D_b, y/D_b) = (0.2, 1.08)$ was the result of a distinct and persistent asymmetry, which was interrelated to this high blockage ratio thinner disk; such a behavior has also been reported and discussed for a similar high blockage ratio single disk configuration by [43].

The maximum non-dimensional axial backflow velocities ($U_{rec,max}/U_{bl}$) and the axial location where these maximum reverse flow velocities are encountered ($X_{rec,max}/D_b$), are also presented in Table 1. The strength of the backflow is important in practical flame stabilizers, since it is directly related to the capacity of the body to promote higher entrainment rates and longer residence times [6,44]. Maximum back flow velocities were found in the cases of the cone shaped and thin disk afterbodies for BR0.48, e.g., C-BR0.48-RIM2, C-BR0.48-RIM3 and D-BR0.48-RIM1. This behavior can be traced to the flow trajectory around the sharper trailing edge angle of these geometries. Both D-BR048-RIM2 and D-BR048-RIM3 induced similar and reduced back-flow velocities, ($U_{rec,max}/U_{bl} = 0.37$), which quickly recovered to positive values at $y/D_b = 0.77$. On the other hand, for the smaller blockage, the minimum reverse flow velocities were produced by the thicker rim disks and particularly the D-BR0.23-RIM3 case ($U_{rec,max}/U_{bl} = 0.31$), while for the cone shaped bodies minimum reverse flow velocities were found for the thicker cone, e.g., C-BR0.23-RIM3 case ($U_{rec,max}/U_{bl} = 0.50$).

Figure 4 displays the locus of the separation streamline, non-dimensionalized with the bluff body diameter of each different afterbody, providing an indication of the impact of the bluntness on the size and placement of the recirculation torus. The position of the separation or zero streamline (ψ) was determined by the following expression:

$$\psi(y, r) = \int_0^r u(y, r) r dr = 0 \quad (1)$$

for several axial measurement stations up to the stagnation point.

The dimensional recirculation lengths were found to increase with baffle diameter, although when non-dimensionalized with the diameter of the baffle, an inverse trend was obtained.

For BR0.23 cases, the largest recirculation zone was established by the C-BR0.23-RIM2 baffle with a length, L, and a width, W, of 1.34 and 1.19 D_b , respectively, with the results of the blunt cone (C-RIM3) and the thin disk (D-RIM1) recirculation sizes following the trend of the C-BR0.23-RIM2 case. On the other hand, D-BR0.23-RIM2 and D-BR0.23-RIM3 bodies have similar RZ sizes, both producing significantly narrower and shorter recirculation boundaries. The above described trends were also followed closely by the BR0.48 baffles. Those trends signify an inverse relationship between the blockage ratio

and the non-dimensional recirculation zone extend, where smaller blockage ratios result in larger recirculation zones, regardless of the studied after body shapes.

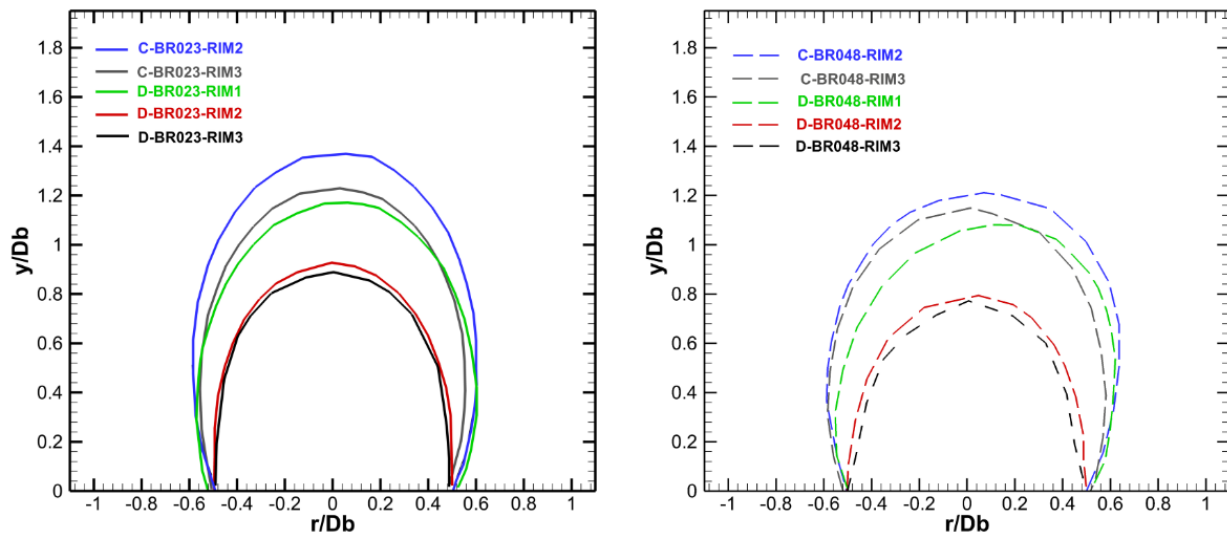


Figure 4. Locus of the separation streamline for each investigated cases.

For cone shaped bluff bodies and smaller thickness disks, the location of the zero-streamline close to the bluff body trailing edge, indicates larger and positive (with respect to axial flow direction) flow deflection angles ranging from 18° to 34° (Table 1), causing a wider spread of the annular jet and of the subsequently developing wake. The thick disk baffles (D-RIM 2 and 3) result in a more streamlined flow with almost negative angles ranging from -2° to -5° , implying a diminishing radial velocity component contribution.

Furthermore, the L/W ratio [4], which represents an approximate measure of the rate of spread of the recirculation zone, is given in Table 1, implying a relative independency from the geometry of the bluff body. More significantly, this ratio was found to decrease by 10–15% when doubling the blockage ratio, by 17–20% as we move from the cone to the disk and by 5% when increasing the bluff body thicknesses.

A synopsis of the inlet conditions and some global performance values related to the near wake results are given in Table 1.

The recirculating mass within the primary zone, \dot{m}_{REC} , has also been determined, using the following equation as described in [38], non-dimensionalized by the inlet air mass through the annular exit plane, \dot{m}_{inlet} :

$$\dot{m}_{REC} = 2\pi \int_0^{r1} \rho_f u(r) dA \quad (2)$$

where, ρ_f is the density of the fluid, u is the axial component of the velocity, r is the distance from the centerline of the bluff body, and $r1$ is the distance from the axis of the bluff body to the eye of the primary vortex (see Figure 2). These values indicate that the RZ size correlates rather satisfactorily with the engulfed recirculating mass [45], apart from the thinner disk cases. Most likely this inconsistency occurs due to the intense asymmetric recirculating wake development in this geometry, a behavior that deteriorates at the larger blockages.

The variations in the flow features, produced by selected representative bluff body geometries, are schematically illustrated in terms of the flow disposition around the afterbody exit plane and within the recirculation region, Figure 5.

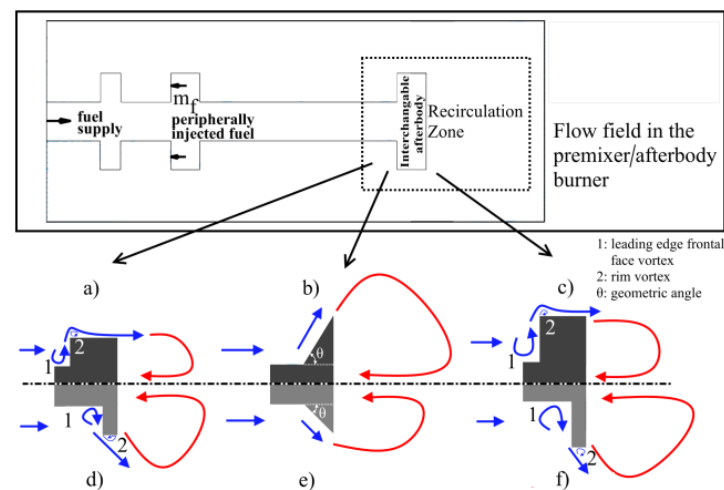


Figure 5. Flow disposition around selected bluff body configurations; (a) D-BR0.23-RIM3, (b) C-BR0.23-RIM2, (c) D-BR0.48-RIM3, (d) D-BR0.23-RIM1, (e) C-BR0.23-RIM2 and (f) D-BR0.48-RIM1.

The leading bluff body face shape and the rim edge play a significant role in determining the flow deflection and re-ingestion within the backflow region. As a result, the emanating flow angle is not always aligned with the geometrical trailing edge angle, as indicated in Table 1.

More specifically, it was observed that in the case of the high blockage cones the shear layer distribution followed the geometrical angle of the baffle, whilst in the smaller blockage ratio cone the shear layer did not appear to be an extension of the geometrical angle. On the other hand, in disk shaped baffles, the exiting flow deflection appeared to be influenced by both rim thickness and blockage. The thinner rim disks appeared to exhibit an inherently unstable shear layer detachment, resulting in a non-uniform circumferential flow ejection angle and the establishment of an asymmetric recirculation. However, in the thicker rim disks (RIM3) the flow angle became almost parallel to the geometrical trailing edge angle.

Moreover, the flow emanating from the disk exit plane is affected by the quality of the flow exiting from the upstream disk cavity formation and the two established toroidal vortices i.e., the leading edge frontal face vortex (1) and the rim vortex (2) [38,46] as depicted in Figure 5. The strength and size of both these vortices depend on the premixing cavity arrangement, the blockage ratio and the rim thickness for the same upstream inlet conditions.

For the thick rim cases, the rim vortex was followed by immediate flow reattachment on the rim length (Figure 5a,c). As the disk thickness narrows, the rim vortex gradually occupies a greater extent of the rim length and its effect on the trailing edge flow angle is augmented. This trend became more pronounced for the thinner rims, where the leading face toroidal vortex, vortex (2), plays a more significant role in defining the flow deflection at the trailing edge (Figure 5d,f). The leading face toroidal vortex (1) implicitly transforms the blunt disk front into a more aerodynamically streamlined forebody shape. On the other hand, the rim vortex creates an effective larger BR than the geometric one and at the same time promotes operation with lower deflection angles. Overall, it is important to distinguish between geometric and aerodynamic bluffness, as the estimation of the former is based on the diameter of the baffle and the estimation of the latter is based on the specific aerodynamic features surrounding the baffle.

All these effects reflect on the efficiency of flow stabilization for each studied configuration, as related to the shear layer deflection, the mass entrainment levels, the pressure drop, the strain rates acting in the near wake region and the possibility of inducing an inherently unstable behavior. These characteristics can be found useful in determining the optimal

configuration for flame stabilization, over a wide range of fuels and mixture compositions, each of which may exhibit individual flame anchoring properties and challenges, i.e., flame speeds and extinction stretches.

To emphasize the significance of the near wake region, flow field properties such as the turbulent kinetic energy and the total and turbulent strains, have been also estimated and compared, along the streamline that encapsulates the recirculating wake region and these are associated with steep gradients of turbulent transport.

The turbulent kinetic energy (TKE) and the mean strain rate (α_m) were determined using the following expressions:

$$TKE/U_{bl}^2 = 0.5 * (2 * x * v'^2 + u'^2) / U_{bl}^2 * 100 \tag{3}$$

$$\alpha_m = \sqrt{2 * [(du/dy)^2 + (dv/dr)^2] + (du/dr + dv/dy)^2} \tag{4}$$

where U_{bl} is the bulk blocked axial velocity and u' and v' the RMS axial and radial velocity components respectively.

The spatial distributions of TKE are illustrated in Figure 6, where the assumption has been made that the azimuthal fluctuating velocity component contribution, w' , is equal to the radial, v' , in this axisymmetric flow.

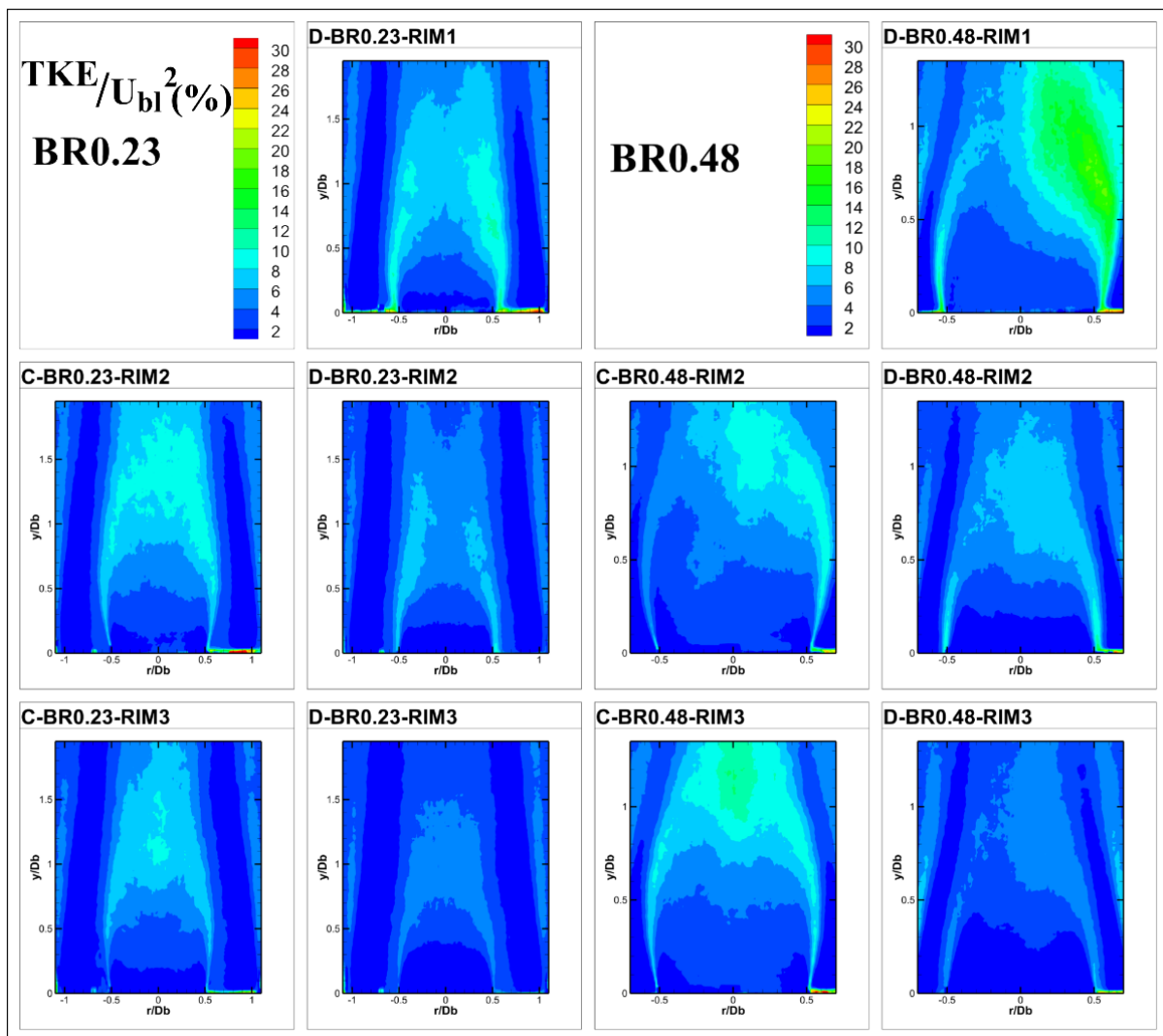


Figure 6. Distributions of normalized TKE contours.

The smaller blockage ratio baffles generally produce lower normalized TKE values than the BR0.48 baffles at levels ranging from 20% to 35%, as a result of lower radial and axial RMS velocity component values. Maximum generation of TKE levels for the disk shaped bodies was identified close to the bluff body trailing rim edge, along the shear layer region, while for the cones maximum levels were encountered in the vicinity of the recirculation zone reattachment region. This distinct difference could be attributed to the higher radial velocity components attained by the cones, at the RZ reattachment position, as a result of the stronger deflection of the shear layer emanating from the cone. Similarly, decreasing the geometrical angle of the cone shaped bodies contributed to a higher accumulation of TKE production in the region at and around the stagnation point. The D-BR0.48-RIM1 case produces a similar trend to the C-BR0.48-RIM2 configuration partly due to the initial higher deflection of the shear layer at the rim edge and partly due to the non-symmetric toroidal vortex formation, which results in an enhanced turbulent activity at the oscillating reattachment position.

Moreover, it becomes apparent that the disk rim thickness plays a significant role in the disposition of the TKE along the wake. For instance, by doubling the rim thickness, from RIM1 to RIM2, the local maxima at the flanking shear layer were reduced by 36% and attained a more cylindrical shape when compared to the thinner disk TKE field. Further moving from RIM2 to RIM3, resulted in a substantial reduction in TKE by about 46%. Comparable results were derived for higher blockage ratio baffles, with peak TKE levels at 18%, 8.5% and 6% for RIM1, RIM2 and RIM3 disks, respectively. Although combustion is known to alter the respective flow fields, the above information could imply that different stabilization and extinction behaviors found in the literature i.e., [7,47] could be partially attributed to the variations in turbulence levels resulting from the geometrical characteristics of the employed stabilization arrangement. Moreover, as the reverse flow region poses a challenge for computational methodologies as well, the above discussion could be valuable in guiding requirements regarding mesh density and turbulence modeling.

Centerline (CL) profiles of the axial and radial velocity root mean square (RMS) fluctuations are also presented in Figure 7, to provide a picture of the turbulent structure of the studied flows.

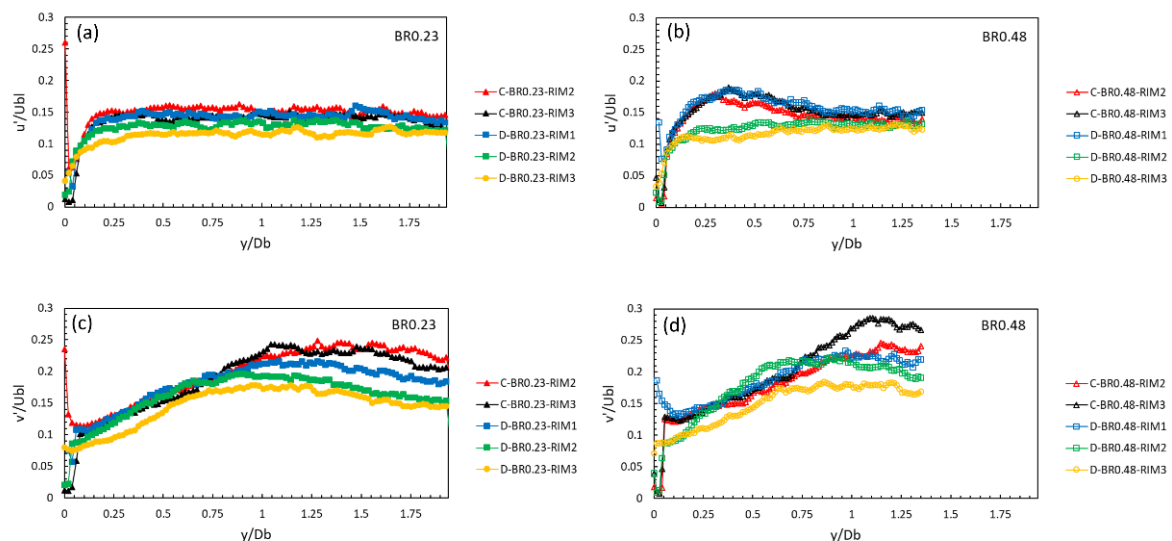


Figure 7. Centerline profiles of the axial (a,b) and radial (c,d), RMS velocity components normalized by U_{bl} (i) BR0.23 and (ii) BR0.48 baffles.

The axial turbulence intensity levels, along the centerline, inside the RZ are nearly uniform, regardless of blockage and bluff body shape. The radial turbulence intensity component attains overall higher values with constant magnitude up to $0.5 D_b$ and decrease as the wake develops further downstream of the reattachment region; this is well

supported by previous findings in the literature [6]. In general, both components display almost uniform distributions along the CL with peak values dominated by regions of local anisotropy encountered in the bluff body trailing edge and the reattachment regions, Figure 7. Finally, thicker rim disks appear to generate lower radial and axial RMS values in contrast to thinner rim disks or cones.

A comparison between the development of the turbulence intensity levels along the centerline, Figure 7, and the zero streamline, Figure 8, permits a better understanding of the interactions between the reverse zone, the externally spreading shear layer and the redevelopment zone, which extends from the reattachment point up to the axial position where the centerline axial velocity achieves its plateau.

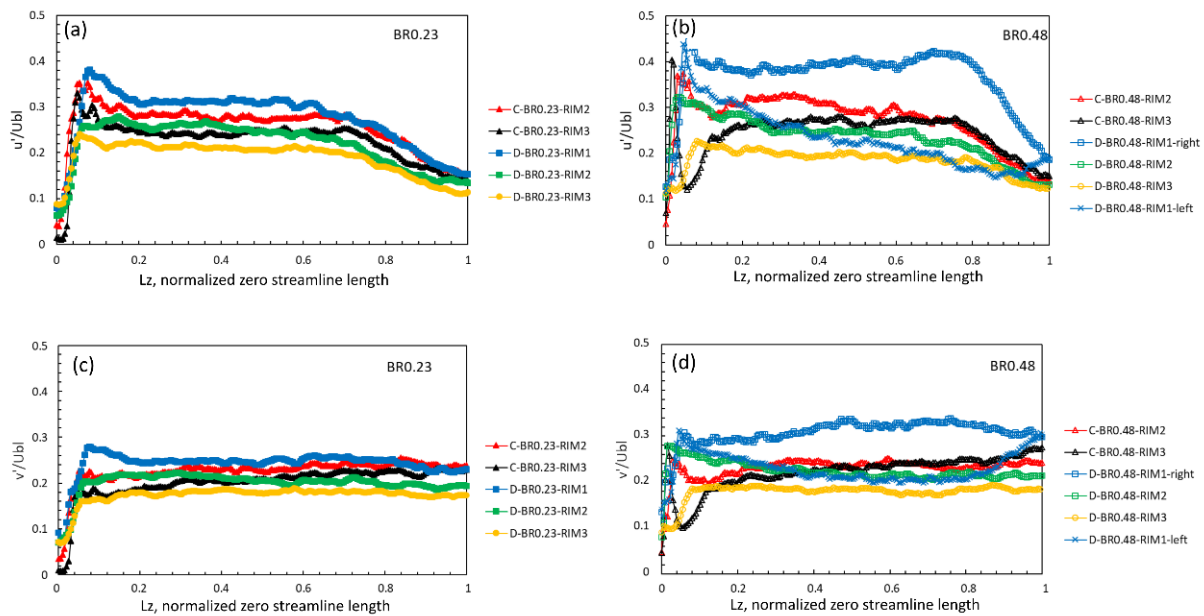


Figure 8. Zero streamline distributions of the axial (a,b) and radial (c,d) velocity fluctuations, for (i) BR0.23 and (ii) BR0.48 baffles.

With reference to the bubble regions designated in Figure 9, the zero streamline on one hand follows closely the emanating shear layer in region 1, half way along the bubble, and on the other hand defines the boundary, where the flow converges toward the reattachment, in region 2. The zero streamline also coincides with peak radial turbulence intensity distributions related to local mixing signifying the entrainment activity and transport across the RZ boundary.

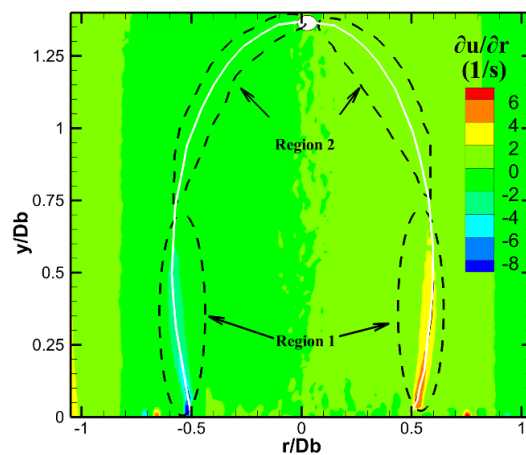


Figure 9. Distributions of $\partial u/\partial r$ (shear layer) at the wake development of C-BR0.23-RIM2 configuration and topology of zero streamline.

Initially, velocity fluctuations reach a peak, close to the baffle edge, at a distance of about 0.05–0.1 along the normalized, by the burner diameter D_b , zero streamline length (L_z), with a subsequent decay followed by a near constant value up to 0.15–0.2 L_z (region 1) and then a sudden drop toward the stagnation location (region 2), Figure 9, [48].

For both blockages higher velocity fluctuations, around 25% in the radial and about 35% in the axial direction, are exhibited by the thinner disks all along the dividing streamline, with the cones falling right below, around 22% and 30% respectively. Lastly, disks with RIMs 2 and 3 achieved values less than 20% for both radial and axial fluctuations.

The strain rate distributions in these fuel–air premixer/flame stabilizer configurations affect drastically the flame placement and stabilization under the counterpart reacting conditions [12,30]. The mean or bulk strain rate (see Equation (4)) topologies have been estimated from the time averaged velocity fields, employing a central differencing scheme for the involved velocity gradients, and are shown in Figure 10 for the ten selected baffles.

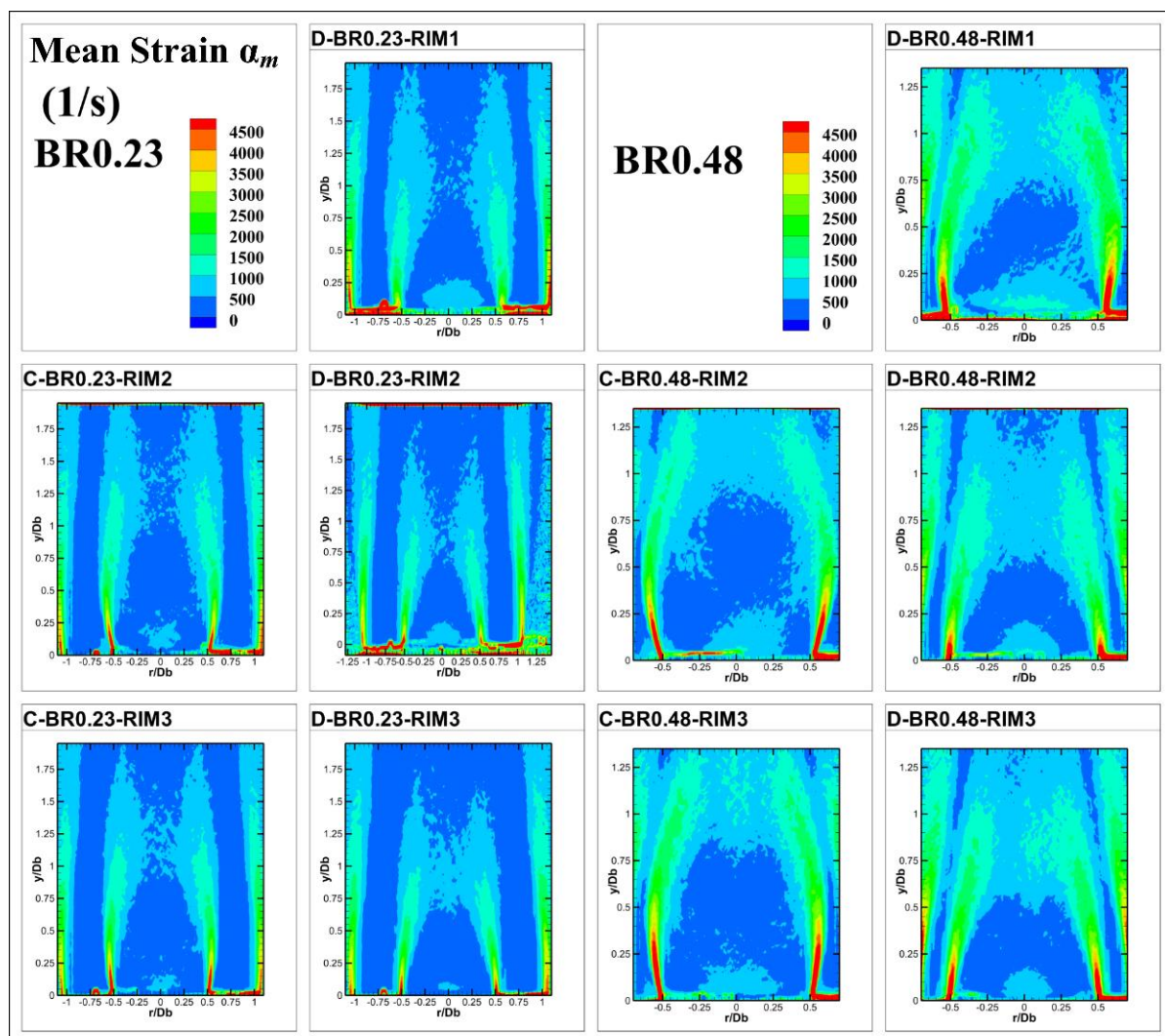


Figure 10. Mean strain rate contours for the examined bluff bodies.

In the vicinity of the bluff body edge the mean strain rate values are higher for larger blockage cones and thinner disks than for the thicker disks and the smaller blockage baffles. This trend could be associated with the increased deflection angles and the accompanying velocity gradients close to the annular exit. A twofold increase in the blockage ratio, sustained a measurable amplification of the mean strain rate production both along the shear layers and closer to the stagnation point.

Comparing bulk strain rate production between baffle shapes, of the same blockage, suggested that the cone produced a strain rate 1.7 times higher than that of the disk. Furthermore, increasing the rim thickness by a factor of two, reduced the bulk strain by a factor of 1.7, for the disk shaped baffles.

A further contribution to the strain rate comes from the smallest turbulence scales. According to [49] the straining by the smallest eddies can be described as the inverse of the Kolmogorov time scale. These eddies can possibly enter into the flame structure and produce the largest straining rates, possibly leading to local extinction of some inner reactions, when considering reacting configurations. Although reactions are expected to alter the specific strain values derived from an isothermal configuration, primarily due to pressure and density changes, the overall trends regarding the different baffle geometries can be usefully projected to assist in the interpretation of the stabilization behavior of different fuels and blends. The turbulent strain rate, α_t , has been derived from the following expressions:

$$\alpha_t = \frac{1}{\tau_k} \quad (5)$$

$$\tau_k = (\nu/\varepsilon)^{1/2} \quad (6)$$

$$\varepsilon = C_\mu(TKE^{3/2}/l_t) \quad (7)$$

where τ_k express the Kolmogorov time scale, ν is the kinematic viscosity of air, ε is the dissipation rate, C_μ is an empirical factor (approximately 0.09), TKE is the turbulent kinetic energy, obtained from Equation (3) and l_t is the integral length scale.

In the present work, the integral length scales were computed from the spatial auto correlation of the PIV data along the longitudinal direction, similar to [12].

$$l_t = \int_0^{h_\infty} R_{ii}(y, r, h) dh \quad (8)$$

where x and y were the radial and axial positions of the point at which the integral lengths were computed. Then, the spatial autocorrelation was estimated from the following equation:

$$R_{ii}(y, r, h) = \frac{\overline{[u(y, r, t) - u(y, r)] [u(y + h, r, t) - u(y + h, r)]}}{\overline{[u(y, r, t) - u(y, r)]^2}} \quad (9)$$

where the overbar represents ensemble averaging and $u(y, r, t)$ represent instantaneous axial velocity values. The autocorrelation function was executed for each cell, associated with the counterpart velocity vector, along the stream-wise direction of the measurement domain, until the “ R ” parameter equaled zero. The produced results are consistent to those reported in the literature [12]. Attention must be paid according to [50], to the spatial measurement domain, which should be large i.e., at least six times lengthier than the integral length scale.

Examining Figure 11, it is evident that the prominent effect of enlarging the bluff body diameter is the growth and spread of the turbulent strain rate levels along the shear layer development and close to the stagnation region. Cone shaped baffles exhibit higher values than the corresponding disks. Additionally, enlarging the rim of disk baffles substantially reduces the magnitude of the turbulent strain rate levels. Specifically, turbulent strain rate magnitude appears to be strongly affected by the rim thickness all along the shear layer development, exhibiting a 40% decrease from RIM1 to RIM3, whilst smaller variations are attained in the reattachment region, of up to 16%, for smaller blockages. Likewise, under the larger blockage conditions, rim lengthening causes a decrease of about 43% at the shear layers and in the stagnation region.

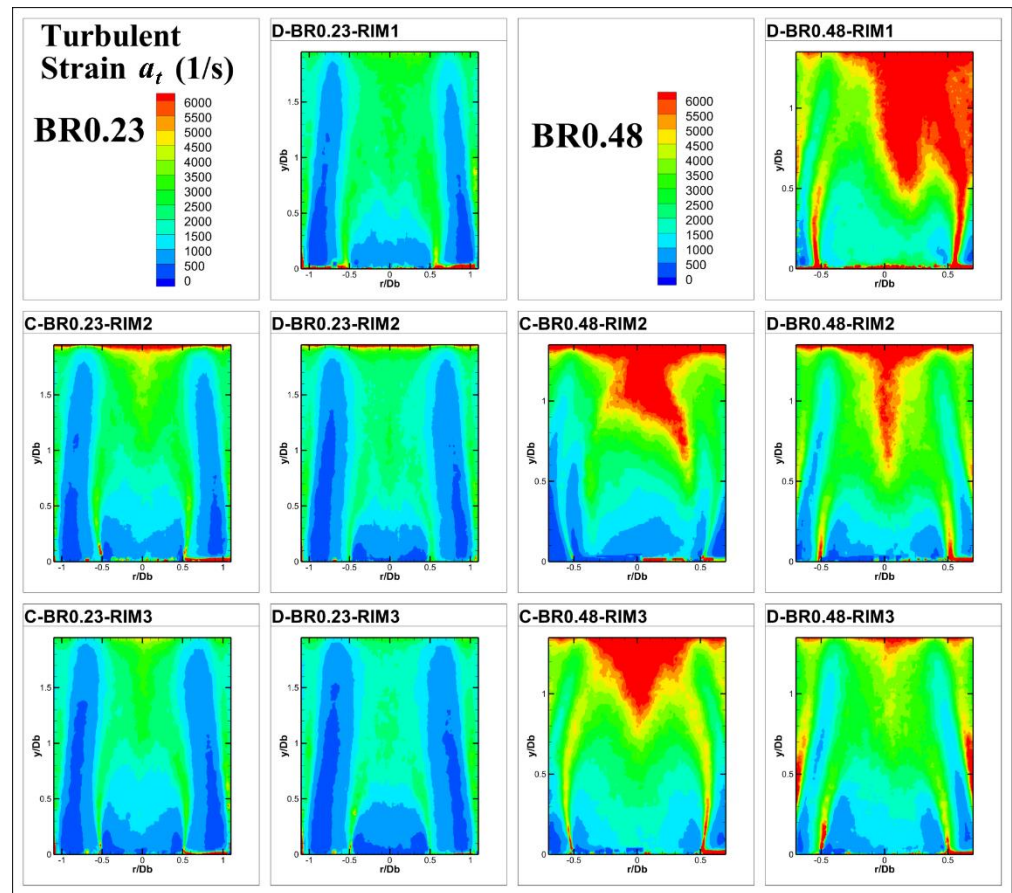


Figure 11. Contours of turbulent strain rate for the examined cases.

In Figure 12, the turbulent and the total strain levels are presented. The total strain rate represents the combined contribution of the mean and turbulent strain rates, plotted along the zero-streamline boundary of the recirculation zone. The assessment of the strain rate fields in the vicinity of the toroidal shear layer, where the incoming fresh mixture is expected to be re-ignited by the recirculating combustion products, on counterpart reacting set ups, would give a rough estimation of the locally anticipated strain rates. The mean strain rate distributions would indicate regions, where the local maxima of aerodynamic strain rate levels could potentially disturb the flame by stretching and wrinkling the flame front. At the same time, the turbulent strain rate distributions could demarcate locations where the smallest turbulent scales are likely to penetrate the reacting front, forcing departures from the flamelet structure and leading to local extinction events, under reaction. Although reactions and heat release may alter, to some extent, the above deductions, projection of the present cold flow structural properties might provide a useful interlink with reacting operation.

The highest values of the turbulent and total strain rates in the initially developing region were achieved in the proximity of the bluff body rim, at $Lz = 0.05\text{--}0.1$, along the trailing edge. In the intermediate region, the strain values diminished monotonically and remained constant, up to the second region, where total strain either attained constant values for small blockages or slightly increased for larger blockages. For smaller blockages, maximum total strain rate values, of about 15,000 and 11,000 1/s, were estimated for C-BR0.23-RIM3 and C-BR0.23-RIM2, respectively. Then, the D-BR0.23-RIM1 case followed with levels of up to 8000 1/s. Subsequently, the strain values declined monotonically up to the reattachment, where the lowest measured values ranged from 2800 to 3200 1/s.

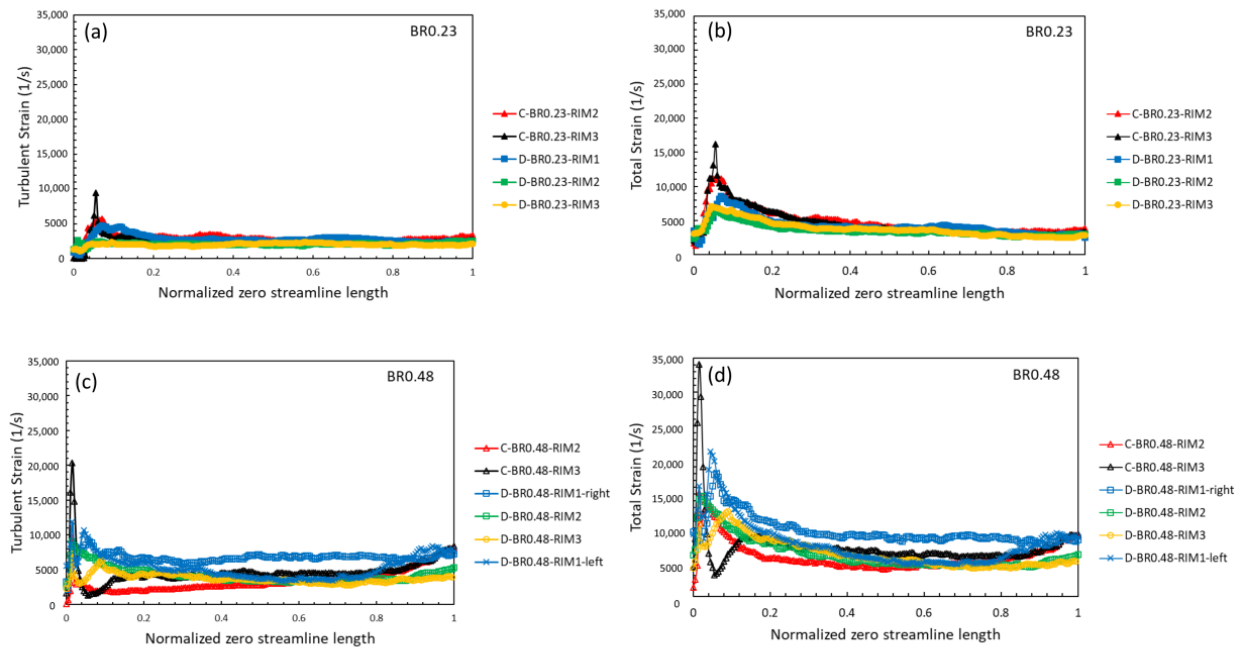


Figure 12. Turbulent (a,c) and total (b,d) strain profiles along zero-streamline for BR0.23 and BR0.48 baffles.

The distributions of the turbulent and total strain rates along the path of the zero-streamline remained qualitatively similar as the blockage of the baffles increased from 23% to 48%, with insignificant discrepancies up to the stagnation region. Quantitatively, the maximum levels of the strain rates for the larger baffles were almost twice those of the respective smaller baffles, with the maximum values for both blockages encountered closer to the lip of the burner rim. This suggests that smaller bodies, and particularly disk shaped ones, could accommodate flame stabilization of fuel-oxidizer mixtures that are less resilient to aerodynamic stretch and have lower extinction stretch values, i.e., a lean heptane–air mixture is more vulnerable to extinction due to aerodynamic stretches than a propane–air mixture, therefore a disk shaped body with a small blockage ratio seems more promising for heptane–air mixture stabilization than a larger blockage ratio cone shaped body, with the same thickness. Nevertheless, such observations can only be of a tentative nature regarding the behavior of a reacting front: flame extinction is a time dependent phenomenon and depends not only on the peak stretch exerted on the flame front but also on the probability for these stretch values to occur and on the relevant turbulent reacting front regime of the specific flame [40].

The effect of rim thickness is more clearly depicted in Figure 12. An increase in thickness from RIM1 to RIM2 caused total strain rate reduction of 25%, while from RIM2 to RIM3 the effect was rather unimportant with changes of only 7% for the smaller blockages, Figure 12b,d. On the other hand, stronger variations were obtained for larger blockages due to increased rim thickness; 20–27% from RIM1 to RIM2 and 17% from RIM2 to RIM3. Trailing edge flows with greater angles raise the aerodynamic total strain, rendering ultra-lean flame stabilization challenging and particularly so for baffles with larger blockage ratios and steeper trailing edge angles. Finally, the contribution of the mean strain to the total strain rate was about 70% and seemed to be dominant in comparison to the turbulent strain, in the front section of the recirculation region (region 1), for all baffles except for disks with high blockages, whereby bulk and turbulent strain participate equally in the stabilization region.

From the investigations performed by the authors, basic characteristics of the cold flow wake such as discussed above, e.g., recirculation lengths, strain fields, turbulence levels and wake recovery rates, maintain their basic properties under combusting conditions, suffering moderate alterations of their important features [30,37,39]. Similar observations

have been reported by related works in the literature i.e., [9,45,51]. Recirculation lengths and entrainment rates are moderately increased for ultra-lean conditions and then gradually reduced as mixtures become richer, with respect to the isothermal case [12,30,51]. Strain fields follow similar trends with the location of the peak values altered due to the reacting shear layer expansion [12,30], while turbulence intensities gradually decrease with mixture strength due to heat release and dilatation effects. [12,30,51]. The relative differences and trends, produced by the individual bluff bodies under cold flow conditions, are expected to be largely maintained under reaction and heat release, for similar inlet mixture stratification. Therefore, although cold flow studies may not be readily extrapolated to the reacting configurations, they remain of great value in elucidating expected trends and variations of counterpart reacting set ups.

6. Summary and Conclusions

In this work, time averaged and turbulent characteristics of the isothermal wake development downstream of a variety of stabilizers were analyzed and discussed. PIV measurements of mean and turbulent quantities have been obtained throughout the near wake region for a range of commonly used bluff body flame stabilizers, operating in conjunction with an upstream premixing section. The results helped to demarcate the range of topologies of the central recirculation zone and of the annular shear layers along quantifying the turbulent characteristics of the developing wake. Detailed measurements along the zero streamline and in the axial and radial directions were obtained to characterize the turbulent transport and the entrainment activity across and within the central recirculation zone for each stabilizer. The results highlighted the impact of the interaction between the baffle trailing edge geometry and the upstream double cavity premixer section, on the afterbody exit velocity characteristics and the different impact between the effective geometric and aerodynamic bluntness of each bluff body. Cone shaped and thinner disk bodies exposed similar characteristics regarding the trailing edge shear layer angle of ejection. Downstream of the cone shaped bluff bodies, and particularly those with the steeper angle, larger recirculation zones were formed, while an increase in the thickness of the disk rim resulted in shorter bubbles. For the same bluff body shape, an increase in blockage ratio produced an attendant increase in the RZ length, while maximum backflow velocities were encountered for the thinner bodies, either of cone or disk shape. Moreover, an increase in BR resulted in higher *TKE* values whilst similar variations in the rim thickness revealed an opposite trend. In general, thicker baffles appeared to be more competent in maintaining a symmetric wake development regardless of blockage ratio. Moreover, along the wake, thicker rims produced lower levels of turbulence intensity, both in the axial and radial directions, with the same trend being encountered across the zero streamline. Thinner disks produced larger strains compared to their thicker counterparts, while cone shaped bluff bodies achieved almost twice the strain rate values of their counterpart disks. Finally, an increase in BR was followed by an attendant growth of the respective strain levels. In general, the thinner disk and the cone shaped bodies presented the most intense wake development with larger and stronger recirculations and elevated turbulence levels, compared to thicker disks. An increase in BR seems to reinforce these trends. The above information combined with the fuel–air mixture wake topologies, obtained in the investigated premixer/burner set ups of [38], provides useful information for the optimization of the counterpart reacting configurations. The suitable choice of flame stabilizer, with respect to specific characteristics of the employed fuel, can also contribute to an optimum operation regarding flame stabilization and extinction behavior for a range of fuels and fuel blends.

Author Contributions: Conceptualization, G.P. and P.K.; methodology, G.P., K.S. and A.N.; formal analysis, G.P. and K.S.; investigation, G.P., K.S. and A.N.; resources, P.K.; writing—original draft preparation, G.P., K.S. and P.K.; writing—review and editing, G.P., K.S. and P.K.; supervision, P.K.; project administration, P.K.; funding acquisition, P.K. All authors have read and agreed to the published version of the manuscript.

Funding: This research received no external funding. The APC was funded by the research Committee of the University of Patras.

Informed Consent Statement: Not applicable.

Data Availability Statement: Not applicable.

Acknowledgments: This publication has been funded by research Committee of the University of Patras.

Conflicts of Interest: The authors declare no conflict of interest.

Appendix A

The uncertainty levels related to the PIV measurements are presented in Figure A1. The estimation procedure has been based on uncertainties arising from the employed equipment, the particle dynamics and the sampling process as analyzed in a previous work of the authors [38].

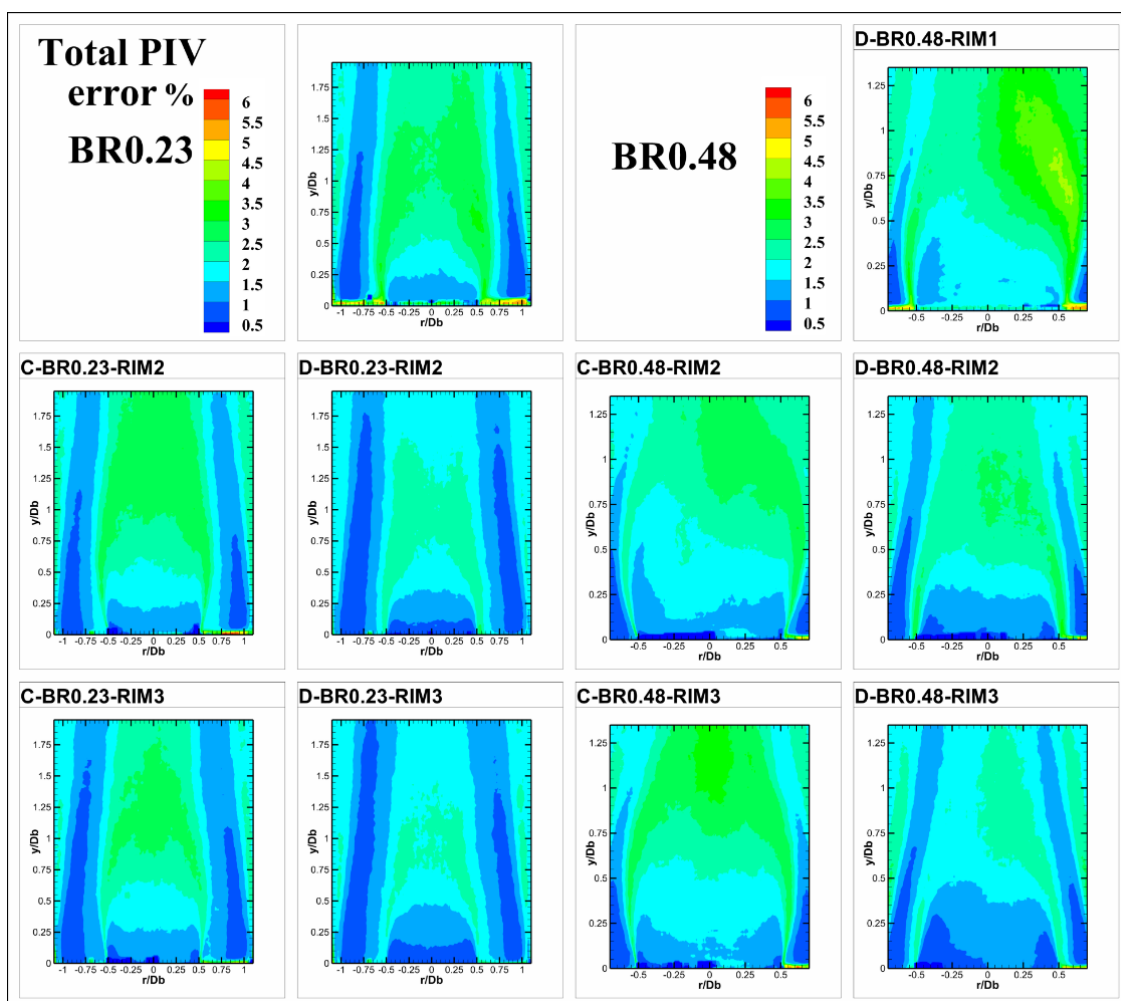


Figure A1. Contours of the total uncertainty in the estimation of velocity due to equipment, particle dynamics and sampling, for all the studied configurations.

Maximum uncertainty levels were obtained for thin disk baffles at the exit plane. Additionally, an error of about 4–5% was estimated at the shear layers and at the stagnation point for cone shaped bluff bodies and thin disks. Lower uncertainty levels, at about 3%, were recorded for thicker rim disks, i.e., RIM2 and RIM3.

References

1. Koenig, K.; Roshko, A. An experimental study of geometrical effects on the drag and flow field of two bluff bodies separated by a gap. *J. Fluid Mech.* **1985**, *156*, 167–204. [[CrossRef](#)]
2. Shanbhogue, S.J.; Husain, S.; Lieuwen, T. Lean blowoff of bluff body stabilized flames: Scaling and dynamics. *Prog. Energy Combust. Sci.* **2009**, *35*, 98–120. [[CrossRef](#)]
3. Bearman, P.W. Challenging problems in bluff body wakes. In *Bluff-Body Wakes, Dynamics and Instabilities*; Springer: Berlin/Heidelberg, Germany, 1993; pp. 1–10. [[CrossRef](#)]
4. Wright, F.H. Bluff-body flame stabilization: Blockage effects. *Combust. Flame* **1959**, *3*, 319–337. [[CrossRef](#)]
5. Esquiva-Dano, I.; Nguyen, H.T.; Escudie, D. Influence of a bluff-body's shape on the stabilization regime of non-premixed flames. *Combust. Flame* **2001**, *127*, 2167–2180. [[CrossRef](#)]
6. Heitor, M.V.; Taylor, A.M.; Whitelaw, J.H. Velocity and scalar characteristics of turbulent premixed flames stabilized on confined axisymmetric baffles. *Combust. Sci. Technol.* **1988**, *62*, 97–126. [[CrossRef](#)]
7. Kariuki, J.; Dawson, J.R.; Mastorakos, E. Measurements in turbulent premixed bluff body flames close to blow-off. *Combust. Flame* **2012**, *159*, 2589–2607. [[CrossRef](#)]
8. Runyon, J.; Marsh, R.; Bowen, P.; Pugh, D.; Giles, A.; Morris, S. Lean methane flame stability in a premixed generic swirl burner: Isothermal flow and atmospheric combustion characterization. *Exp. Therm. Fluid Sci.* **2018**, *92*, 125–140. [[CrossRef](#)]
9. Sweeney, M.S.; Hochgreb, S.; Barlow, R.S. The structure of premixed and stratified low turbulence flames. *Combust. Flame* **2011**, *158*, 935–948. [[CrossRef](#)]
10. Cheng, L.; Spencer, A. Residence time measurement of an isothermal combustor flow field. *Exp. Fluids* **2012**, *53*, 647–661. [[CrossRef](#)]
11. Xiouris, C.Z.; Koutmos, P. Fluid dynamics modeling of a stratified disk burner in swirl co-flow. *Appl. Therm. Eng.* **2012**, *35*, 60–70. [[CrossRef](#)]
12. Souflas, K.; Koutmos, P. On the non-reacting flow and mixing fields of an axisymmetric disk stabilizer, under inlet mixture stratification and preheat. *Exp. Therm. Fluid Sci.* **2018**, *99*, 357–366. [[CrossRef](#)]
13. Wang, J.; Zhang, C.; Gu, S.; Yang, K.; Li, H.; Lai, Y.; Yurchenko, D. Enhancement of low-speed piezoelectric wind energy harvesting by bluff body shapes: Spindle-like and butterfly-like cross-sections. *Aerosp. Sci. Technol.* **2020**, *103*, 105898. [[CrossRef](#)]
14. Lam, K.; Zou, L. Experimental study and large eddy simulation for the turbulent flow around four cylinders in an in-line square configuration. *Int. J. Heat Fluid Flow* **2009**, *30*, 276–285. [[CrossRef](#)]
15. Tong, Y.; Liu, X.; Chen, S.; Li, Z.; Klingmann, J. Effects of the position of a bluff-body on the diffusion flames: A combined experimental and numerical study. *Appl. Therm. Eng.* **2018**, *131*, 507–521. [[CrossRef](#)]
16. Bakrozis, A.G.; Papailiou, D.D.; Koutmos, P. A study of the turbulent structure of a two-dimensional diffusion flame formed behind a slender bluff-body. *Combust. Flame* **1999**, *119*, 291–306. [[CrossRef](#)]
17. Caetano, N.R.; Figueira da Silva, L.F. A comparative experimental study of turbulent non premixed flames stabilized by a bluff-body burner. *Exp. Therm. Fluid Sci.* **2015**, *63*, 20–33. [[CrossRef](#)]
18. Chaudhuri, S.; Cetegen, B.M. Blowoff characteristics of bluff-body stabilized conical premixed flames with upstream spatial mixture gradients and velocity oscillations. *Combust. Flame* **2008**, *153*, 616–633. [[CrossRef](#)]
19. Dawson, J.R.; Gordon, R.L.; Kariuki, J.; Mastorakos, E.; Masri, A.R.; Juddoo, M. Visualization of blow-off events in bluff-body stabilized turbulent premixed flames. *Proc. Combust. Inst.* **2011**, *33*, 1559–1566. [[CrossRef](#)]
20. Barlow, R.S.; Dunn, M.J.; Magnotti, G. Preferential transport effects in premixed bluff-body stabilized CH₄/H₂ flames. *Combust. Flame* **2015**, *162*, 727–735. [[CrossRef](#)]
21. Barlow, R.S.; Dunn, M.J.; Sweeney, M.S.; Hochgreb, S. Effects of preferential transport in turbulent bluff-body-stabilized lean premixed CH₄/air flames. *Combust. Flame* **2012**, *159*, 2563–2575. [[CrossRef](#)]
22. Zhou, R.; Balusamy, S.; Sweeney, M.S.; Barlow, R.S.; Hochgreb, S. Flow field measurements of a series of turbulent premixed and stratified methane/air flames. *Combust. Flame* **2013**, *160*, 2017–2028. [[CrossRef](#)]
23. Paterakis, G.; Souflas, K.; Dogkas, E.; Koutmos, P. A comparison of the characteristics of planar and axisymmetric bluff-body combustors operated under stratified inlet mixture conditions. *J. Combust.* **2013**, *2013*, 860508. [[CrossRef](#)]
24. Karagiannaki, C.; Paterakis, G.; Souflas, K.; Dogkas, E.; Koutmos, P. Performance evaluation of a model swirl burner under premixed or stratified inlet mixture conditions. *J. Energy Eng.* **2015**, *141*, 1–9. [[CrossRef](#)]
25. Kuenne, G.; Seffrin, F.; Fuest, F.; Stahler, T.; Ketelheun, A.; Geyer, D.; Janicka, J.; Dreizler, A. Experimental and numerical analysis of a lean premixed stratified burner using 1D Raman/Rayleigh scattering and large eddy simulation. *Combust. Flame* **2012**, *159*, 2669–2689. [[CrossRef](#)]
26. Meares, S.; Masri, A.R. A modified piloted burner for stabilizing turbulent flames of inhomogeneous mixtures. *Combust. Flame* **2014**, *161*, 484–495. [[CrossRef](#)]
27. Galley, D.; Ducruix, S.; Lacas, F.; Veynante, D. Mixing and stabilization study of a partially premixed swirling flame using laser induced fluorescence. *Combust. Flame* **2011**, *158*, 155–171. [[CrossRef](#)]
28. Masri, A.R. Partial premixing and stratification in turbulent flames. *Proc. Combust. Inst.* **2015**, *35*, 1115–1136. [[CrossRef](#)]
29. Galizzi, C.; Escudié, D. Experimental analysis of an oblique turbulent flame front propagating in a stratified flow. *Combust. Flame* **2010**, *157*, 2277–2285. [[CrossRef](#)]

30. Souflas, K.; Perrakis, K.; Koutmos, P. On the turbulent flow and pollutant emission characteristics of disk stabilized propane-air flames, under inlet mixture stratification and preheat. *Fuel* **2020**, *260*, 116333. [[CrossRef](#)]
31. Baxter, M.R.; Lefebvre, A.H. Weak extinction limits of large scale flameholders. *Proc. ASME Turbo Expo* **1991**, *3*, 776–782. [[CrossRef](#)]
32. Miao, J.J.; Leu, T.S.; Liu, T.W.; Chou, J.H. On vortex shedding behind a circular disk. *Exp. Fluids* **1997**, *23*, 225–233. [[CrossRef](#)]
33. Esquivia-Dano, I.; Escudié, D. A way of considering the influence of the bluff-body geometry on the nonpremixed flame stabilization process. *Combust. Flame* **2005**, *142*, 299–302. [[CrossRef](#)]
34. Masri, A.R.; Dally, B.B.; Barlow, R.S.; Carter, C.D. The structure of the recirculation zone of a bluff-body combustor. *Symp. Combust.* **1994**, *25*, 1301–1308. [[CrossRef](#)]
35. Kundu, K.M.; Banerjee, D. Theoretical analysis on flame stabilization by a bluff-body. *Combust. Sci. Technol.* **1977**, *17*, 153–162. [[CrossRef](#)]
36. Koutmos, P.; Paterakis, G.; Dogkas, E.; Karagiannaki, C. The impact of variable inlet mixture stratification on flame topology and emissions performance of a premixer/swirl burner configuration. *J. Combust.* **2012**, *2012*, 374089. [[CrossRef](#)]
37. Karagiannaki, C.; Dogkas, E.; Paterakis, G.; Souflas, K.; Psarakis, E.Z.; Vasiliou, P.; Koutmos, P. A comparison of the characteristics of disk stabilized lean propane flames operated under premixed or stratified inlet mixture conditions. *Exp. Therm. Fluid Sci.* **2014**, *59*, 264–274. [[CrossRef](#)]
38. Paterakis, G.; Politi, E.; Koutmos, P. Experimental investigation of isothermal scalar mixing fields downstream of axisymmetric baffles under fully premixed or stratified inlet mixture conditions. *Exp. Therm. Fluid Sci.* **2019**, *108*, 1–15. [[CrossRef](#)]
39. Xiouris, C.; Koutmos, P. An experimental investigation of the interaction of swirl flow with partially premixed disk stabilized propane flames. *Exp. Therm. Fluid Sci.* **2011**, *35*, 1055–1066. [[CrossRef](#)]
40. Souflas, K.; Koutmos, P. Effects of stratification and preheat on turbulent flame characteristics and stabilization. *Flow Turbul. Combust.* **2021**, 1–26. [[CrossRef](#)]
41. Paterakis, G.; Koutmos, P. Effect of modulation of the inlet velocity and equivalence ratio gradients on the stabilization of stratified axisymmetric bluff-body flames. *J. Combust.* **2018**, *2018*, 6581345. [[CrossRef](#)]
42. Stafford, J.; Walsh, E.; Egan, V. A statistical analysis for time-averaged turbulent and fluctuating flow fields using Particle Image Velocimetry. *Flow Meas. Instrum.* **2012**, *26*, 1–9. [[CrossRef](#)]
43. Del Taglia, C.; Blum, L.; Gass, J.; Ventikos, Y.; Poulidakos, D. Numerical and experimental investigation of an annular jet flow with large blockage. *J. Fluids Eng. Trans. ASME* **2004**, *126*, 375–384. [[CrossRef](#)]
44. Whitelaw, J.H. Velocity characteristics in the turbulent near wakes of confined axisymmetric bluff bodies. *J. Fluid Mech.* **1984**, *139*, 391–416.
45. Taylor, A.M.K.P. Confined Isothermal and Combusting Flows behind Axisymmetric Baffles. Ph.D. Thesis, University of London, London, UK, 1982.
46. Paterakis, G. Experimental Investigation of Isothermal and Reacting Flow Characteristics Downstream of Axisymmetric Bluff Body Stabilizers under Stratified or Fully Premixed Inlet Mixture Conditions. Ph.D. Thesis, University of Patras, Patras, Greece, 2020.
47. Chowdhury, B.R.; Cetegen, B.M. Effects of free stream flow turbulence on blowoff characteristics of bluff-body stabilized premixed flames. *Combust. Flame* **2018**, *190*, 302–316. [[CrossRef](#)]
48. Chen, R.H.; Driscoll, J.F. The role of the recirculation vortex in improving fuel-air mixing within swirling flames. *Symp. Combust.* **1989**, *22*, 531–540. [[CrossRef](#)]
49. Peters, N. Laminar flamelet concepts in turbulent combustion. *Symp. Combust.* **1988**, *21*, 1231–1250. [[CrossRef](#)]
50. O'Neill, P.L.; Nicolaides, D.; Honnery, D.R.; Soria, J. Autocorrelation functions and the determination of integral length with reference to experimental and numerical data. In Proceedings of the Fifteenth Australasian Fluid Mechanics Conference, Sydney, Australia, 13–17 December 2004.
51. Pan, J.C.; Vangsness, M.D.; Ballal, D.R. Aerodynamics of bluff-body stabilized confined turbulent premixed flames. *J. Eng. Gas. Turbines Power* **1992**, *114*, 783–789. [[CrossRef](#)]